SPIN-PHONON TRANSITION PROBABILITIES FOR Cr^{3+} in RUBY

ABSTRACT

Measurements of X-band spectra of ruby samples with different Cr^{3+} concentration, grown by the "vapor phase" method, were carried out at 9.3 Kmc. The angular variations of the spin-lattice relaxation times of the samples were measured using the pulse saturation technique and at helium temperature.

An experimental method based on a technique of microwave pumping, described by Weissfloch (1966), was used in this work to measure spin-phonon transition probabilities in ruby. The results indicate the existence of relaxation processes which cannot be related to the spin-lattice coupling parameters obtained from ultrasonic and static stress experiments.

Eaton Electronics Research Laboratory
Department of Physics
January 1970

Mostafa I. El-Azab
M.Sc.

SPIN-PHONON TRANSITION PROBABILITIES FOR Cr^{3+} in RUBY

by

Mostafa I. El-Azab

A thesis submitted to the

Faculty of Graduate Studies and Research

in partial fulfilment of the requirements for the

Degree of Master of Science

Eaton Electronics Research Laboratory
Department of Physics
McGill University
Montreal 110, P.Q.

January 1970

INDEX

ABSTRACT

Measurements of X-band spectra of ruby samples with different Cr^{3+} concentration, grown by the "vapor phase" method, were carried out at 9.3 Kmc. The angular variations of the spin-lattice relaxation times of the samples were measured using the pulse saturation technique and at helium temperature.

An experimental method based on a technique of microwave pumping, described by Weissfloch (1966), was used in this work to measure spin-phonon transition probabilities in ruby. The results indicate the existence of relaxation processes which cannot be related to the spin-lattice coupling parameters obtained from ultrasonic and static stress experiments.

ACKNOWLEDGEMENTS

The author wishes to thank Professor C.F. Weissfloch who supervised the research, for many helpful comments and invaluable criticisms, and Dr. G. Lichtenberger for numerous stimulating discussions.

Sincere thanks are due to several members of the staff and students of the Eaton Electronics Research Laboratory, some of whom are no longer there.

This research project was supported by grants from the Defence Research Board and the National Research Council. Such financial assistance is gratefully acknowledged.

I. Introduction

Early experimental work on the return of a paramagnetic ion to thermodynamic equilibrium with the host lattice, i.e. paramagnetic relaxation, was carried out by non-resonant methods, which yield data averaged over the energy levels of the measured sample. This early work has been summarized in a book by Gorter (1947). The advent of paramagnetic resonance has made it possible to study, in more detail, processes associated with different energy levels of a paramagnetic sample. Presently, several methods for the determination of paramagnetic relaxation times are available, including the steady state saturation method (Bloembergen,1948), pulse saturation technique (Bowers and Mims, 1959) and the resonance-dispersion method (Carruthers and Rumin, 1965).

Theoretical work in paramagnetic resonance starts as early as 1932, when Waller published his analysis of the coupling resulting from the modulation of the spin-spin interaction by the vibrations of the lattice. Later, Kronig (1939) and Van Vleck (1940) calculated quantitatively the relaxation mechanism involving the modulation of the crystal field by the vibrating lattice, both for the Kramers doublet ions with spin of one half, and for the ions with zero field splitting of the energy levels of the ground state. In recent years Stevens (1967) recast the relaxation theory to take

full advantage of the development of crystal-field techniques; part of his work will be reviewed in Chapter II.

An experimental technique for investigating the direct spin-lattice coupling involves injecting phonons, in a narrow frequency range, into a paramagnetic crystal, and observing their interaction with the spin system. Shiren and Tucker (1961) determined the angular variation of the transition probabilities and compared them with those predicted by Van Vleck's theory. The result was a confirmation of the general aspects of this theory. The first spin-lattice coupling constant, corresponding to the coupling between the Cr^{3+} spins of ruby and the longitudinal waves travelling on the C-axis of the crystal, was measured by Tucker (1961) by using an ultrasonic attenuation method. Further work by Shiren (1962) and Watkins and Feher (1962) has shown that the static stress measurement of these coupling constants gives results of the same magnitude as the ultrasonic work, and in addition, provides the absolute sign of the coupling.

In few cases, spin-lattice relaxation times have been calculated starting from simpler physical parameters, such as the spin-lattice coupling constants (G-tensor). The well-known case of such an attempt is that of ruby, where the spin-lattice coupling constants (G-tensor) were measured by Donoho and Hemphill (1962) and Hemphill, Donoho and McDonald (1966), and the corresponding spin-lattice relaxation times computed by Donoho (1964). This thesis is concerned with the study of the spin-lattice relaxation of Cr^{3+} in ruby.

Standley and Vaughan(1965) reported good agreement between the angular dependence of the relaxation time for the 2-3 and 3-4 transitions predicted by Donoho (1964), and their measurements on the so-called "vapor-phase" ruby, at X-band. For ruby grown by the standard Verneuil technique, no such agreement was observed.

This agreement in angular dependence, in spite of the fact that the measured relaxation times were found to be shorter by a factor of 2 than the predicted ones, seemed to show rather convincingly that the relaxation in "vapor-phase" ruby was in this case governed by the pure spin-lattice process. Later measurements of relaxation times versus angle at 35 GHz (Lees, Moore and Standley 1967) showed only fair agreement with the computed angular dependence and shed some doubt on the conclusions reached on the basis of the experimental data at X-band. For better understanding of spin-lattice relaxation mechanisms in "vapor-phase" grown ruby, further experimental investigation and a comparison of the results obtained with the presently accepted theoretical model were carried out and are reported in the following chapters.

Chapter II of this thesis reviews the necessary theoretical background for the subsequent experimentation. Theory of spin-lattice relaxation, spin-phonon transition probabilities, and relaxation rate equations are included in that review. Measurements of X-band spectra and angular dependence of relaxation time at liquid He temperature for ruby are reported in Chapter III. An

experimental method based on a technique of microwave pumping described by Weissfloch (1966) was used in this work to measure spin-phonon transition probabilities in ruby (Chapter IV). Discussion of the results obtained and the conclusion drawn are presented in Chapter V.

II. Theory of Spin-Lattice Relaxation

II. 1 Paramagnetic resonance.

The state of a paramagnetic ion placed in a host lattice can be described by a Hamiltonian of the form

$$\mathcal{H} = H_o + V + H_{so} + H_z + H_{ol} \qquad 2.1$$

where the first term represents the free ion energy, the second, the crystalline binding energy, H_{so} and H_z the spin-orbit term and Zeeman term of the electrons outside the filled shells. H_{ol} is the Kronig-Van Vleck orbit lattice energy which is held responsible for the phenomenon of spin-lattice relaxation. The terms omitted from (2. 1) which are of less importance in our case, are those such as spin-spin, nuclear Zeeman, and quadruple effects.

When calculating the energy levels of the paramagnetic ground state, the spin-Hamiltonian formalism is commonly used. Detailed discussion of such formalism and spin-Hamiltonian coefficients for several ions in different lattice can be found in several articles, such as that of Bleaney and Stevens (1953) and that of Bowers and Owen (1955).

In the case of ruby (Cr^{3+} ion in Al_2O_3), the spin-Hamiltonian has axial symmetry, and is given by

$$H = g_{\parallel} H_z S_z + g_{\perp} (H_x S_x + H_y \cdot S_y) + D [S_z^2 - {}^1/_3 S(S+1)] \qquad 2.2$$

with the numerical constants published by Manenkov and Prokhorov (1955), Geusic (1956), and Zaripov and Shamonion (1956) as follows

$$2D = -11.493 \pm .006 \text{ Kmc}$$

$$g_{\parallel} = 1.9840 \pm .0006$$

$$g_{\perp} = 1.9867 \pm .0006$$

II.2 Spin-Lattice relaxation

The fundamental mechanisms of spin-lattice relaxation in dilute iron group were explained in the work of Kronig(1939) and Van Vleck (1940). In this model a paramagnetic ion in a crystal lattice is considered to be subjected to the electric field formed by the neighbouring ions, and when the lattice vibrates, the interionic distances are modulated at the frequency of the lattice vibrations. The last term of equation (2.1) represents a perturbation of the original Hamiltonian due to such modulation of the crystalline field. With such a perturbation a spin-transition occurs.

The energy transfer takes place principally by two mechanisms, namely, a direct process in which a spin absorbs, or emits, a phonon of energy equal to the energy separation between two levels, and a Raman process where two phonons, with energy difference

equal to such separation, are involved. At low temperature the direct process is predominant.

The theory of spin-phonon transition probabilities is treated in the next section (II. 3). The rate equations governing transitions between different energy levels are found in section (II. 4).

II. 3 Spin-Phonon transition probabilities for the one-phonon process.

In this section an outline of the calculation of spin-phonon transition probabilities will be given. For a more detailed discussion, reference is made to Weissfloch (1966), Donoho (1964) and the original work of Van Vleck. The wave lengths of phonons that participate in paramagnetic relaxation are much longer than the interatomic distances. The strain (e) induced by such phonons of wave vector $\vec{K}$ and polarization p is:

$$e_{\kappa\lambda}(\vec{K}, p) = (h/8M\omega)^{1/2} \cdot (a_p^+(\vec{K}) - a_{-p}(\vec{K})) \cdot (p_\kappa K_\lambda + p_\lambda K_\kappa) e^{i\vec{K}.r} \qquad 2.3$$

where

M is the mass of the crystal and a_p^+ and a_p are creation and annihilation operator respectively, with the properties:

$$a_p^+ \mid n_p > \; = (n_p + 1)^{1/2} \mid n_p + 1 >$$

$$a_p \mid n_p > \; = (n_p)^{1/2} \mid n_p - 1 >$$

Van Vleck originally derived the spin-lattice interaction Hamiltonian as a spin operator quadratic in spin and linear in strain. Watkins and Feher (1962) showed that the effect of a small displacement of the ligands on the eigenstate of a paramagnetic ion may be described by a perturbation term, H_{sl}, in the spin-Hamiltonian. For $S > 1/2$, the term is given as:

$$H_{sl} = \Sigma_{\alpha,\beta} D_{\alpha\beta} S_\alpha S_\beta$$

where

S_α, S_β are the conventional pure spin operators, and the tensor (D) is related to strain linearly as follows:

$$D_{\alpha\beta} = \Sigma_{\alpha,\beta,\kappa,\lambda} G_{\alpha\beta\kappa\lambda} \cdot e_{\kappa\lambda}$$

hence

$$H_{sl} = \Sigma_{\alpha,\beta,\kappa,\lambda} G_{\alpha\beta\kappa\lambda} \cdot e_{\kappa\lambda} \cdot S_\alpha \cdot S_\beta \qquad 2.4$$

The tensor G has many of the symmetry properties of the elastic

stiffness tensor, limiting, therefore, the number of independent components. Such components can be evaluated by observing changes in the E.S.R. spectrum when a known stress is applied. Experimental G tensor in the case of Cr^{3+} in ruby was obtained by Donoho (1964), as shown in table Ia.

The phonon-induced transition probability between two spin states, S_i and S_j, with an energy difference $\hbar\omega_{ij}$, due to phonons of angular frequency ω, is given by a time dependent perturbation theory as:

$$W''_{ij} = 2\pi/\hbar \,|\langle S_i, n_p(\vec{K}) \pm 1 | H_{sl} | S_j, n_p(\vec{K})\rangle|^2 \delta(\hbar\omega_{ij} - \hbar\omega)$$

$$= \sum_{\kappa,\lambda} 2\pi/\hbar \,|\langle S_i | H_{\alpha,\lambda} | S_j \rangle|^2 |\langle n_p(\vec{K}) \pm 1 | e_{\kappa\lambda} | n_p(\vec{K})\rangle|^2 \delta(\hbar\omega_{ij} - \hbar\omega) \qquad 2.5$$

where

$$H_{\kappa\lambda} = \sum_{\alpha,\beta,\kappa,\lambda} G_{\alpha\beta\kappa\lambda} S_\alpha \cdot S_\beta$$

Using formulae 2.4 and 2.5 one finds for phonon annihilations that:

$$W''_{ij} = |\langle S_i | H_{\kappa\lambda} | S_j \rangle|^2 (n_p(\vec{K})/8M\omega) | p_\kappa K_\lambda + p_\lambda K_\kappa |^2 \qquad 2.6$$

TABLE Ia.

G Tensor for Ruby

"Symmetry D_{3d} "

G_{11}	G_{12}	$-\frac{1}{2}G_{33}$	G_{14}	$-G_{25}$	G_{16}
G_{12}	G_{11}	$-\frac{1}{2}G_{33}$	$-G_{14}$	G_{25}	$-G_{16}$
$-(G_{11}+G_{12})$	$-(G_{11}+G_{12})$	G_{33}	0	0	0
G_{41}	$-G_{41}$	0	G_{44}	G_{45}	G_{52}
$-G_{52}$	G_{52}	0	$-G_{45}$	G_{44}	G_{41}
$-G_{16}$	G_{16}	0	G_{25}	G_{14}	$\frac{1}{2}(G_{11}-G_{12})$

with the values

$G_{11} = 124.6$, $G_{41} = -15.0$

$G_{12} = -35.8$, $G_{25} = 45.0$

$G_{33} = 181.2$, $G_{52} = 45.0$

$G_{44} = 54.0$, $G_{16} = 0$

$G_{14} = -15.0$, $G_{45} = 0$

where all values are in GC/sec.

where

$n_p(\vec{K})$ is the occupation number of phonons of frequency ω given by Bose-Einstein statistics as:

$$n_p(\vec{K}) = (e^{\hbar\omega/KT} - 1)^{-1} \qquad 2.7$$

In the calculation of spin-lattice transition probabilities, the density of phonon states is required. For phonons with wave vector within solid angle $d\Omega$, this density is given by the expression:

$$\rho(E) = V\omega^2 d\Omega / 8\pi^3 \hbar V^3_{p(\vec{K})} \qquad 2.8$$

where

V is the crystal field potential and $V_{p(\vec{K})}$ is the phase velocity of the wave.

Using equations 2.6, 2.7, and 2.8, one can show that the total transition probability per unit solid angle is of the form:

$$W'_{ij} = F(\omega, T) \sum_p \int |\langle S_i | H_{\kappa\lambda} E_{\kappa\lambda} | S_j \rangle|^2 d\Omega / V^5_p(\vec{K}) \qquad 2.9$$

where

$$E_{\kappa\lambda} = p_\lambda K'_\lambda + K'_\lambda p_\kappa$$

with K' as the unit vector in direction of $\vec{K}$ such that

$$\vec{K}_\lambda = \omega / V_p(\vec{K})\, K'_\lambda$$

and the integral carries over all directions of $\vec{K}$ of the wave vector.

The function $F(\omega, T)$ is given by:

$$F(\omega, T) = V\omega^3 / 32\pi M\hbar \cdot 1/(e^{\hbar\omega/KT} - 1)$$

for spin transition from a lower to an upper state resulting in the annihilation of phonon, and should be replaced by:

$$F'(\omega, T) = F(\omega, T)\, e^{\hbar\omega/KT}$$

for the opposite case. Equation 2.9 may be expanded in the form:

$$W_{ij} = F(\omega, T) G_{\alpha\beta\kappa\lambda} G_{\alpha'\beta'\mu\upsilon} E_{\kappa\lambda\mu\upsilon} \langle S_i | H_{\kappa\lambda} | S_j \rangle \langle S_j | H_{\mu\upsilon} | S_i \rangle \qquad 2.10$$

where

$$E_{\kappa\lambda\mu\upsilon} = \sum_p \int E_{\kappa\lambda} E_{\mu\upsilon} d\Omega / (V_p(\vec{K}))^5 \qquad 2.11$$

Van Vleck (1940) assumed, as an approximation to evaluate the integral 2.11, that the crystal is isotropic, i.e. the acoustic phonons conform to Debye's model of one longitudinal mode of phase velocity V_l and two transverse modes of phase velocity V_t, and that all directions of propagation and polarization have equal

probability. Weissfloch (1966) calculations yield the following values of the three independent $\bar{E}$-coefficients:

$$\bar{E}_{11} = 16\pi/15\ (3/V_l^5 + 2/V_t^5)$$

$$\bar{E}_{12} = 16\pi/15\ (1/V_l^5 - 1/V_t^5)$$

$$\bar{E}_{44} = 8\pi/15\ (2/V_l^5 + 3/V_t^5)$$

The calculations of the spin-phonon transition probabilities are seen to involve a fifth power of phase velocities, which makes it very difficult to obtain meaningful absolute values for the W_{ij}, and hence we shall concern ourselves with relative magnitude only.

II.4 Relaxation rate equations.

In this section, the rate equations governing the change of the energy level populations will be discussed and a solution for these equations will be derived under certain pumping conditions. The derived solution will be used in Chapter IV to evaluate the results of an experiment designed to measure the spin-phonon transition probabilities.

Figure 1(a) shows the population diagram under thermal equilibrium condition, in which case the population of the energy levels will be distributed according to Boltzmann equation. In the

presence of an intense microwave magnetic field of the proper frequency ($h\nu$ equal to energy separation between any two levels), a steady state distribution of the kind shown in Figure 1 (b, c, d) would be achieved. This is simply due to a net upward transition which continues until equalization of the two levels involved is reached. In this case, the pair of levels is said to be saturated.

The next section will deal with a simple two-level system. A four-level system will be considered in section II.4.2.

II .4.1 Rate equations for two-level systems:

(Case of S = 1/2 spin system)

For simplicity, we shall consider this case first. The rates at which relaxation transitions occur in each direction between the spin levels can be given, in general, by upward and downward transition probabilities U_{21} and U_{12} per spin per unit time. In other words, the probability per unit time that a spin in level 2 will make a transition to level 1 is U_{21} and the total number of upward transitions is thus $U_{21}n_2$, with a corollary statement holding for the opposite direction. From these transition probabilities, one can write rate equations governing the time rate of change of the level populations n_2 and n_1 as follows:

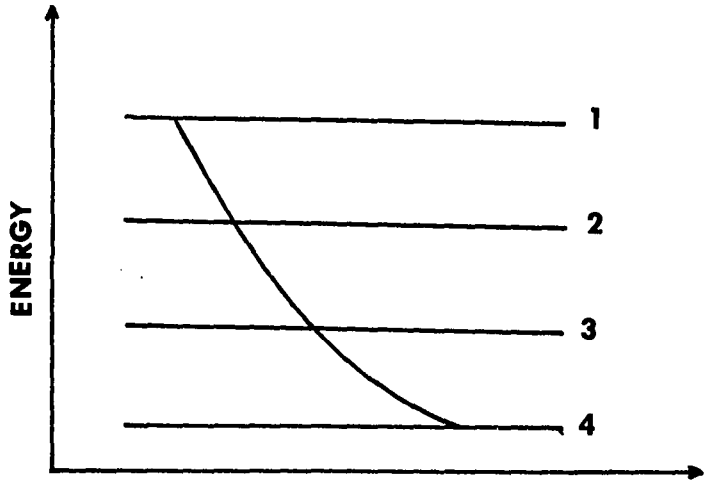

Fig. 1(a)

Energy level population diagram showing thermal equilibrium distribution (Boltzmann distribution)

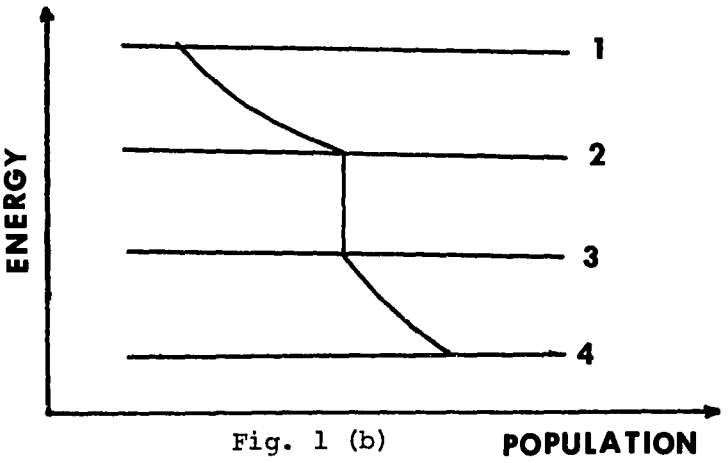

Fig. 1 (b)

Population in presence of radiation of frequency υ_{23} (out of equilibrium)

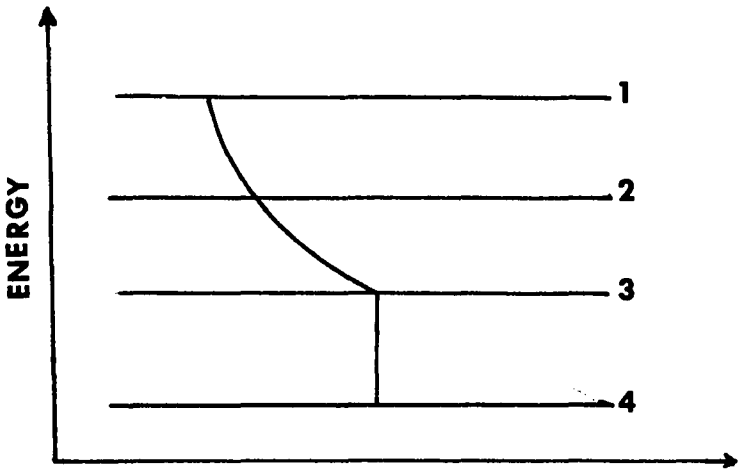

Fig. 1(c)

Steady state population distribution in presence of radiation of frequency υ_{34}

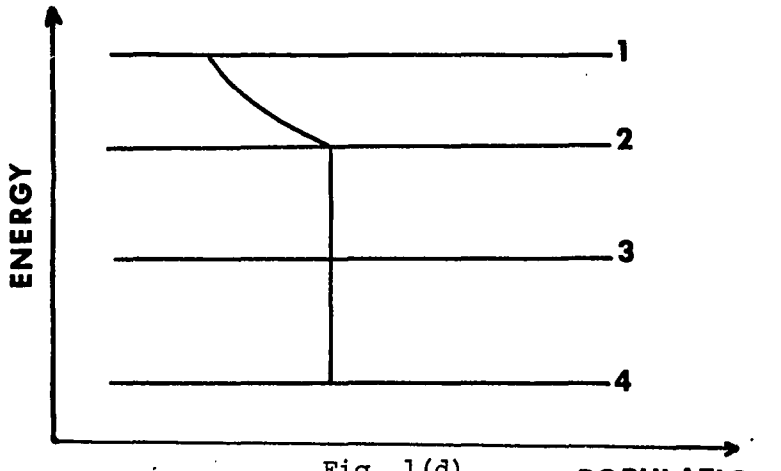

Fig. 1(d)

Steady state population distribution in presence of radiation of frequency υ_{34} and υ_{23}

$$\dot{n}_2 = -U_{21} n_2 + U_{12} n_1$$

$$\dot{n}_1 = U_{21} n_2 - U_{12} n_1 \qquad 2.13$$

The first equation asserts that the time rate of change of the population in level 2 is given by the rate of arrival minus the rate of departure. Similar argument applies for the second equation. One notices that the rate equations automatically fulfill the obvious requirement that dN/dt = 0, i.e., conservation of spins. In equation 2.13, U's represent both the spin-phonon transitions probabilities (W's) and the microwave radiation induced transition probabilities (P's).

At thermal equilibrium and with no microwave radiation present, the level populations must, by definition, be in static equilibrium. Therefore, putting $n_1 = N_1$ and $n_2 = N_2$ into the relaxation rate equation must lead to

$$\dot{n}_2 - \dot{n}_1 = 0$$

Inspection of eq. 2.13 shows that this will be the case only if the relaxation transition probabilities obey the condition

$$W_{12} / W_{21} = N_2 / N_1 = e^{h\upsilon_{12}/KT} \qquad 2.14$$

where

K is Boltzmann constant

T is temperature

h is Plank's constant

υ_{12} is frequency separation between levels 1 and 2

The downward relaxation transition probability, W_{12}, must always turn out to be larger than the upward transition probability, W_{21}, by just the Boltzmann's ratio, if thermal equilibrium is to be maintained.

When the system is subject to radiation field and then the radiation was switched off, the system would return to thermal equilibrium with a relaxation time constant T_1 given by

$$T_1 = (W_{12} + W_{21})^{-1} \qquad 2.15$$

The time constant T_1 is commonly termed the spin-lattice relaxation time.

It is important to notice that induced (absorption) transition probability P_{21} is equal to (emission) transition probability P_{12} and that they both are directly proportional to the power level of the applied r.f. field.

II.4.2 Rate equations for multilevel systems:

(spin system with $S > 1/2$)

The rate equations for any arbitrary level i, including all possible relaxation terms and stimulated transition to all other levels j , can be written as

$$dn_i/dt = \sum_j (U_{ji} n_j - U_{ij} n_i) \qquad 2.16$$

along with the condition

$$\sum_i n_i = \text{constant}$$

which reduces the number of equations in 2.16 by one. The solution for the return to equilibrium of the populations of levels 1 and 2 after a pulse of r.f. power sufficient to saturate the pair of levels, is given in case of four levels as

$$n_1 - n_2 \,/\, n_{10} - n_{20} = 1 - A_1 \exp(-t/T_1) - A_2 \exp(-t/T_2) - A_3 \exp(-t/T_3) \qquad 2.17$$

where n_{10}, n_{20} are thermal equilibrium population values of levels 1 and 2 respectively, and each of the time constants T_1, T_2, and T_3 is a complicated combination of the W_{ij}'s. More generally, the number of time dependent terms is one less the number of levels.

II.4.3 A solution of the rate equations under pumping conditions.

Consider the rate equations (2.16) in the case of a four-level system. If one saturates levels 2-3 and 3-4 with intense microwave radiation of the proper frequencies, the following conditions would be imposed (see Fig. 1d),

$$n_4 = n_3 \quad \text{and consequently} \quad \dot{n}_4 = \dot{n}_3$$

$$n_3 = n_2 \quad \text{and} \quad \dot{n}_3 = \dot{n}_2$$

along with the previous condition

$$n_1 + n_2 + n_3 + n_4 = N \qquad \text{or} \qquad \dot{n}_1 + \dot{n}_2 + \dot{n}_3 + \dot{n}_4 = 0$$

Therefore, the rate equations for such a case would be written explicitly as

$$\dot{n}_4 = \dot{n}_2 = (W_{34}+P_{34}+W_{24}-W_{43}-P_{43}-W_{42}-W_{41})n_2 + (W_{14})n_1$$

$$\dot{n}_3 = \dot{n}_2 = (W_{43}+P_{43}+W_{23}+P_{23}-W_{34}-P_{34}-W_{32}-P_{32}-W_{31})n_2 + (W_{13})n_1 \qquad 2.18$$

$$\dot{n}_2 = (W_{42}+W_{32}+P_{32}-W_{24}-W_{23}-P_{23}-W_{21})n_3 + (W_{12})n_1$$

$$\dot{n}_1 = (W_{41}+W_{31}+W_{21})n_2 + (-W_{14}-W_{13}-W_{12})n_1$$

along with the condition

$$3n_2 + n_1 = N$$

which could be written as

$$n_1 = N - 3n_2$$

By adding the first three relations of equation (2.18) and substituting the value $n_1 = N-3n_2$ into the resulting equation, a differential equation is obtained. Using the solution of this differential equation, one can show, for the 1-2 transition, that the difference in population between level 2 and level 1 is given by the relation

$$n_2 - n_1 = \frac{(W_{14}-W_{41}+W_{13}-W_{31}+W_{12}-W_{21})}{(W_{41}+3W_{14}+W_{31}+3W_{13}+W_{21}+3W_{12})} N \qquad 2.19$$

and the time constant for relaxation to dynamic equilibrium, after a saturating pulse of the 1-2 transition, is given by a single time constant $(T_R)_{21}$, as

$$(T_R)_{21}^{-1} = 1/3\,(W_{41}+3W_{14}+W_{31}+3W_{13}+W_{21}+3W_{12}) \qquad 2.20$$

III. Spectroscopic and relaxation measurements of Cr^{3+} ion in ruby

III. 1 The Paramagnetic Sample Cr^{3+} in Al_2O_3(Ruby).

Ruby is a species of corundum, α-Al_2O_3, colored red by dissolved chromium. Corundum crystallizes in the rhombohedral (sometimes called trigonal) system, with the structure as shown in Fig. 2. The rhombohedral angle is $\alpha = 55^{o}17'$ and the length of the unit cell, $a_o = 5.42^{o}A$. The unit cell contains two Al_2O_3 units. At low concentrations, the Cr^{3+} ion isomorphically displaces the Al^{3+} ion, whose lattice site has trigonal symmetry about the crystalline C axis. This trigonal crystalline field gives Cr^{3+} a single orbital ground state, four-fold degenerate as to spin. The $\lambda(\vec{L}\cdot\vec{S})$ perturbation partially removes this degeneracy to two two-fold degenerate spin levels in zero magnetic field. Applying a D.C. magnetic field would remove completely the degeneracy, resulting in a four-level system. The spin-Hamiltonian for ruby has been derived by several authors and was given in the previous section (eq. 2.2).

Extensive data on the energy levels of ruby have been presented by Chang and Siegman (1958), and Schulz du Bois (1959).

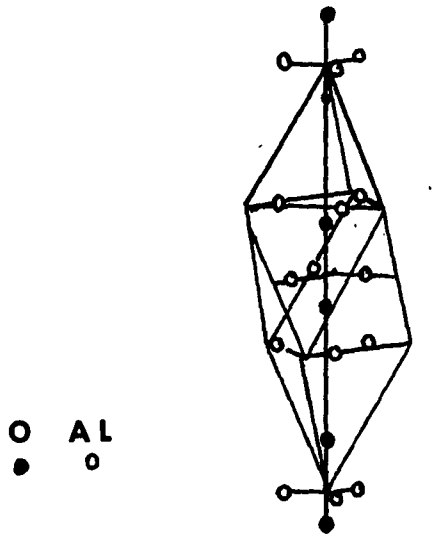

Fig. 2

CORUNDUM CRYSTAL STRUCTURE

Growth of Crystals: synthetic ruby are made by several methods, among them:

1 - The Verneuil or flame process: the starting material is a fine powder consisting of calcining alum ($NH_4Al(SO_4)_2$-$12H_2O$) with chromic oxide (Cr_2O_3). The furnace utilizes an oxyhydrogen flame. The oxides are fed into the flame and the resulting molten crystallizes in boule on a seed-crystal below the flame tip. The boule must be carefully annealed to remove internal stress introduced during growth.

2 - The so-called "vapor-phase" modification of the Verneuil process, developed by Thermal Syndicate Limited. This method involves feeding aluminum and chromium into the flame as halide vapors rather than as solid oxides.

3 - The fluxed-melt technique: The ruby crystals grow from a solution of the oxides in lead oxide/lead fluoride flux.

III. 2 X-band Spectrometer and associate instrumentation.

An ESR spectrometer essentially consists of four main parts:

a. the microwave section includes radiation source, microwave bridge with the sample cavity and compensation network,

b. the receiver with its amplifiers and recording units,

c. the magnet and its stabilized power supply,

d. a cryostat system for low temperature work.

For detailed study of different types of spectrometers and their essential parts, reference is made to books such as the one by Poole (1967) and the M.I.T. Radiation Laboratory series.

The ESR spectrometer, used in this experiment, operated in the X-band and is patterned after apparatus described by Feher (1957). The main microwave oscillator was a klystron (a Varian V-58) that oscillated at 9300.00 megahertz. It provided a power of 500 milliwatts. The output of the klystron was stabilized using a Curry McLaughlin and Len Inc. model 1/F crystal controlled phase-locking unit capable of giving a frequency stability better than 1 part in 10^5. The ruby sample was placed into a two-port cavity of low Q-value, for reasons to be apparent later. This is shown in Fig. 3. For a description of the two-port cavity, refer to Weissfloch (1964).

The microwave power, reflected from the cavity,

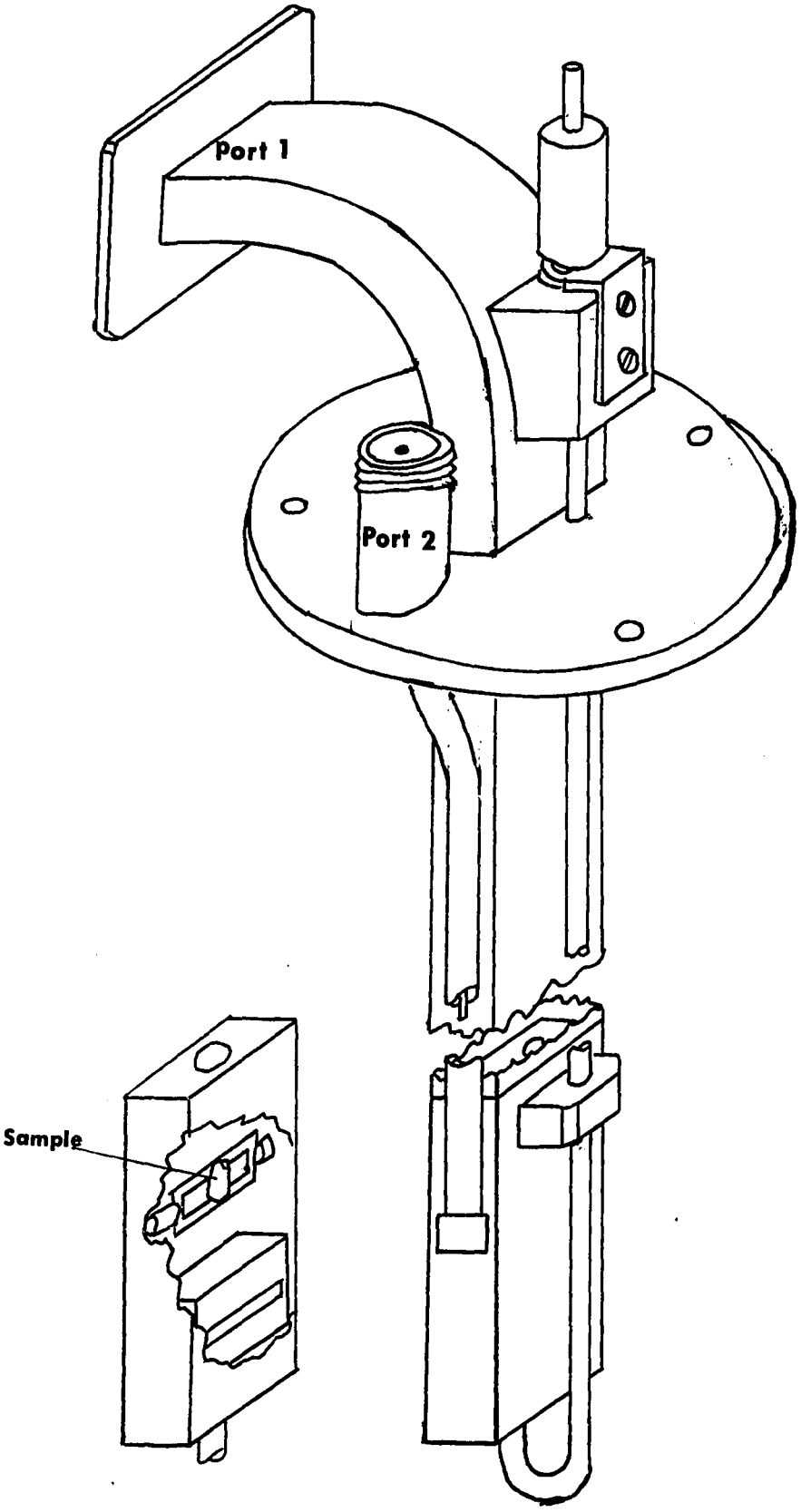

Fig. 3

The two-port spectrometer cavity

entered a balanced mixer where it was mixed with another microwave power from the local oscillator klystron model 2K-39. The frequency of the local oscillator was adjusted at 9330.00 megahertz and was stabilized by a Pound stabilization system. The Pound stabilizer, (Pound 1946, 1947), is designed to maintain the klystron at a minimum difference in frequency from a standard reference cavity. In addition, it removes the frequency deviations occurring at audio-frequencies and those higher which are normally found in the output power of a microwave oscillator. The long term stability of the stabilized oscillator is almost completely determined by the stability of the reference cavity. The 30-mc IF-frequency produced by the mixer, which is the difference between the frequency of the local oscillator and the main klystron, was then amplified by an IFI (Instruments for Industry Inc.) type P 205 A preamplifier. Following this amplifier, a variable attenuator was used to prevent overloading of the subsequent IFI type M-235 IF amplifier and rectifier unit. Both the preamplifier and the amplifier were tuned to produce a 3 megahertz band with center frequency at 30 megahertz. When audio-magnetic field modulation was employed, the signal was further filtered, amplified and phase-sensitively detected for recorder output. The sensitivity of the whole system is estimated by the number of spins detectable. The system could detect 10^{15} spins of DPPH at 77^{o}K with an incident power of 1 μW.

For the relaxation time measurements by pulse saturating technique, the saturating power was switched by a set of Somerset X-400/16 switching diodes, driven by a Tektronix waveform generator and a pulse amplifier. The monitor power was controlled by an attenuator in a by-pass around this microwave switch. The IF-amplifier saturation recovery problems were prevented by a paralysis of the IF-stage during the saturation pulse. This was accomplished by using a second pulse synchronized with the first one. The rectified and filtered output from the 30 mc IF-amplifier was observed and photographed on an oscilloscope screen. The oscilloscope display was triggered by the same pulse which was used to paralyse the amplifier, while a third pulse generator delivered a second trigger to the oscilloscope after completion of the return to equilibrium of the system in order to supply a base line for reference. This base line proved convenient for more accurate measurements on weak lines in the presence of hum. The overall response time of the system was about 50μsec., which have been adequate for measuring the comparatively long relaxation time for ruby. Linear operation of the IF-amplifier rectifier system was insured by plotting the relation between the input vs. the output levels and by choosing the right range where the relation was linear.

Typical optimum signal-to-noise ratio for pulse relaxation measurement on a small sample (2 x 5 x 7 mm) of ruby with 0.05% Cr^{3+} at 4.2°K was 50: 1, allowing accurate relaxation measurements.

Sources of noise include boiling of helium and liquid air coolent, first stage of the IF-preamplifier and some 60 cycle interference.

The chart of the recorder was calibrated in terms of magnetic field for accurate spectroscopic work.

Magnetic Field:

The applied D.C. magnetic field was supplied by a 12" Pacific Electric Motor magnet giving up to 12,000 gauss (with 3" gap) with excellent homogeneity. The magnet could be rotated about the vertical axis to allow angular variation measurements. The stabilizing system used maintained the field constant to within $\pm$ 0.1 gauss over a period of a few minutes and to 1 gauss over a period of a few hours. The field strength was determined by using a nuclear magnetic resonance (NMR) gauss meter (Harvey Wells model E 502), with the probes mounted on the pole faces, and a frequency counter (Hewlett Packard 524B). The magnetic field must be modulated for spectroscopic studies, therefore two additional coils were fixed on the magnet's poles to modulate the steady field. The modulation frequency was 200 hertz and the amplitude of the modulation was set at 0.9 gauss, which was much smaller than the line width of the ruby samples under investigation.

The Cryostat System:

To permit working at very low temperature (liquid He 4.2°K), the cryostat system consists of a glass dewar filled with liquid helium, in which the resonant cavity is immersed, and an outer glass dewar filled with liquid air which prevents excessive evaporation of the helium.

Fig. 4 presents a Block diagram of the ESR spectrometer and some instruments which will be discussed in the next chapter.

III.3 Paramagnetic Spectra of Cr^{3+} in Ruby.

The spectrum of the four transitions of Cr^{3+} in ruby was measured at 9.300 $\pm$ 0.001 GHz as a function of orientation and strength of the applied magnetic field. All measurements were repeated on several samples with different concentrations ranging from .003 to .08% of Cr^{3+} (analyzed by Technical Service Laboratories, Toronto, Ont.). The measured spectra was compared with the published data (e.g. Schulz-DuBois 1959) and agreement was found within the limit of experimental error. Primarily, the spectra was compared with the published data to help in aligning ruby crystals for subsequent experimentation.

Fig. 5 is a plot showing, for a sample (size 2 x 5 x 7 mm) cut from a ruby crystal of .02% Cr^{3+} content, resonance fields as functions of the angle between the crystalline axis and the applied

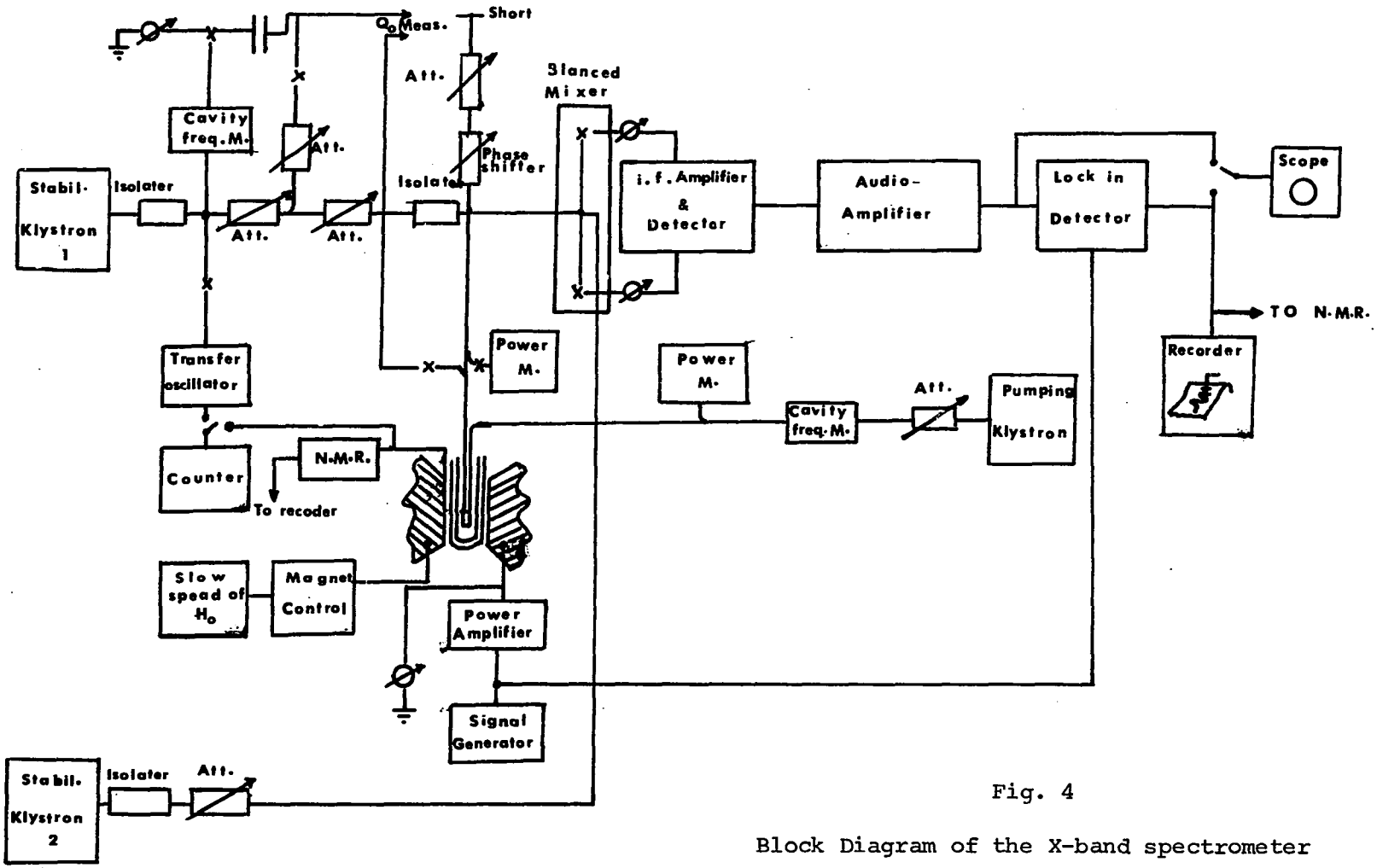

Fig. 4

Block Diagram of the X-band spectrometer

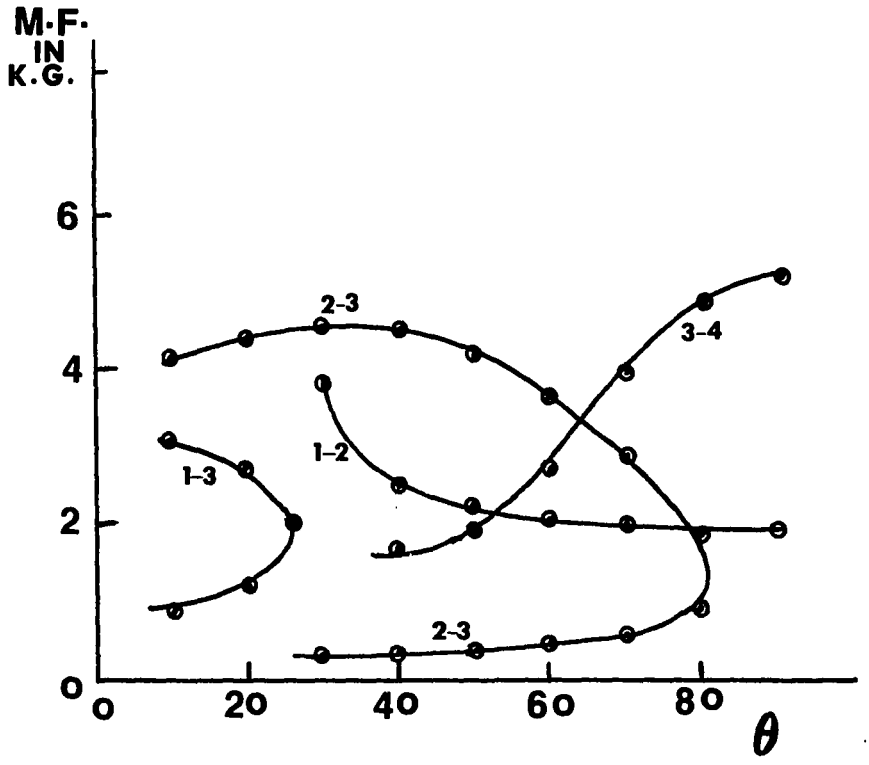

o our measurement

— Schulz-DuBois (1959)

Fig. 5

Angular variation of different transitions of Cr^{3+} in Ruby at 9.3 GC/sec.

$T = 4.2^{o}K$

field. The sample was mounted in the cavity using silicone vacuum grease and the orientation was checked by observing the symmetry of the ESR spectrum at liquid helium temperature. In the same figure, the published data of Schulz-DuBois (1959) are shown (solid line).

The magnetic field in the center of the line was measured using the NMR technique and the derivative of the line was recorded on the recorder unit. A typical line width was of the order of 30 gauss.

III.4 Pulse technique measurements on Ruby.

The spin-lattice relaxation times were measured by the pulse saturation technique (Bowers and Mims 1959). The two levels under consideration were exposed to microwave power pulse of the proper resonant frequency. Then, the saturating power was shut off and the return of the populations to their equilibrium values was monitored on an oscilloscope. The ESR signal was observed using a low power level. The observed relaxation curves were photographed and analysed by reproducing them on a semi-logarithmic graph. The measurements were standardized arbitrarily by defining the relaxation time, for the experimental curves as well as the computed ones, as the time constant of the single exponential which gave the best fit over the first 80% of the amplitude

of the true curve. By carefully choosing the instant at which the oscilloscope trace was photographed, drift, instability and helium boiling effect were minimized. The ruby samples used in the relaxation measurements were the same ones used for spectroscopic results.

All relaxation measurements were carried out on the absorption part of the magnetic susceptibility by setting the magnetic field to the center of the transition under investigation. Measurements were taken at liquid helium temperature (4.2^{o}K) and at frequency equal to 9.3 GC/sec. In most of the cases, only one time constant was extracted. In few cases traces of more than one time constant were observed.

It is of interest to mention here that, theoretically, we expect to have three time constants (as discussed in section II.4) but experimentally, it is difficult to resolve the relaxation curves to its three exponential components.

Angular dependence of the relaxation time:

The variation of relaxation time with crystal orientation for three different transitions was experimentally investigated and compared with the results of theoretical investigation by Donoho (1964). Donoho's results were numerically constructed in such a way as to give what would be expected experimentally. This was done using an IBM 360 computer which calculates the change

in signal strength, as function of time, from the relation

$$n/n_o = 1 + A_1 e^{-t/\tau_1} + A_2 e^{-t/\tau_2} + A_3 e^{-t/\tau_3} \qquad 3.1$$

where

A_1, A_2, A_3, τ_1, τ_2, and τ_3 were taken from theoretical calculations of Donoho

and finds a single time constant best describing the resulting curve.

Figs. 6, 7, and 8 show the experimental results of the angular dependence of the relaxation times for the (1-2), the high field (2-3) and (3-4) transitions respectively; also shown in every case are the experimental points of Standley and Vaughan (1965) and the relaxation times deduced from Donoho's computations which, following the latter, have been scaled down by a factor of two. The scaling down was done to facilitate the comparison with the experimental results since, as mentioned earlier, it is very difficult to obtain meaningful absolute values for the transition probabilities and hence the relaxation times. The scatter in the individual observations were about 15% in the relaxation time measurements, the error in the average, however, is smaller depending on the number of readings taken and the strength of the signal considered. In Table I, a representative value of the relaxation times is given along with the expected range of error for each case and other published data (Standley and Vaughan 1965).

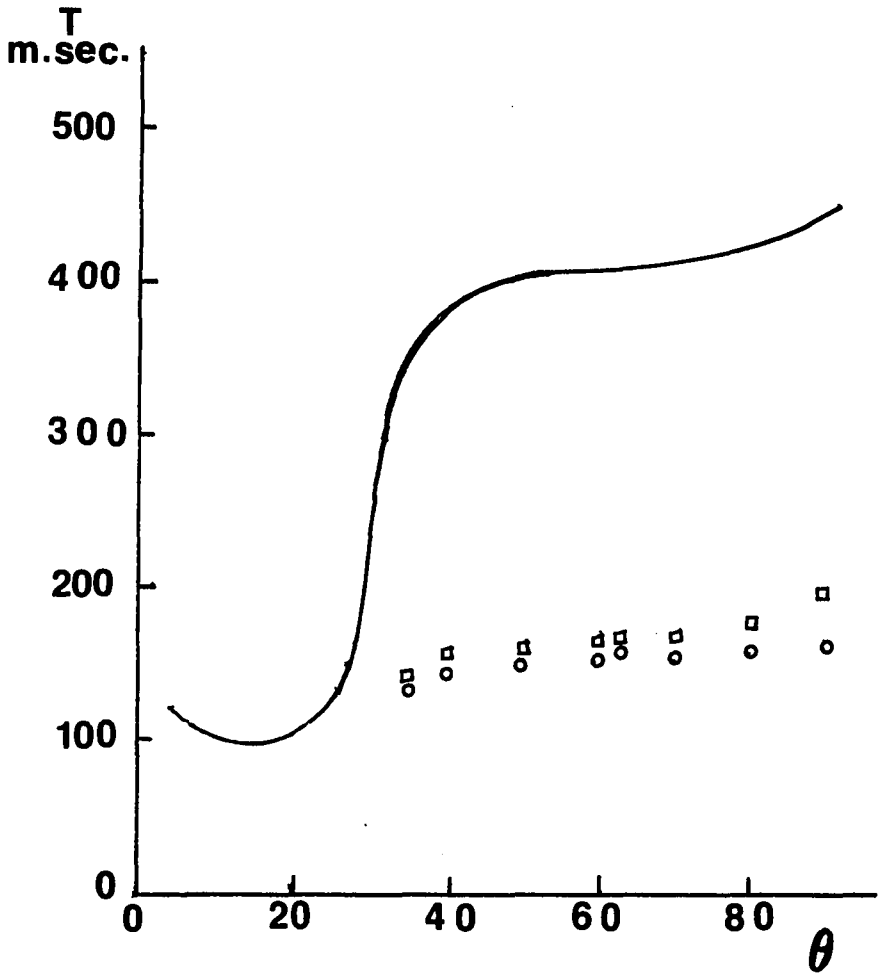

Fig. 6

Relaxation time versus θ for 1-2 transitions.

Full line represents theoretical curve scaled down by a factor of 2. ✖ Standley and Vaughan (1965).

○ and □ our measurements for samples I and II respectively.

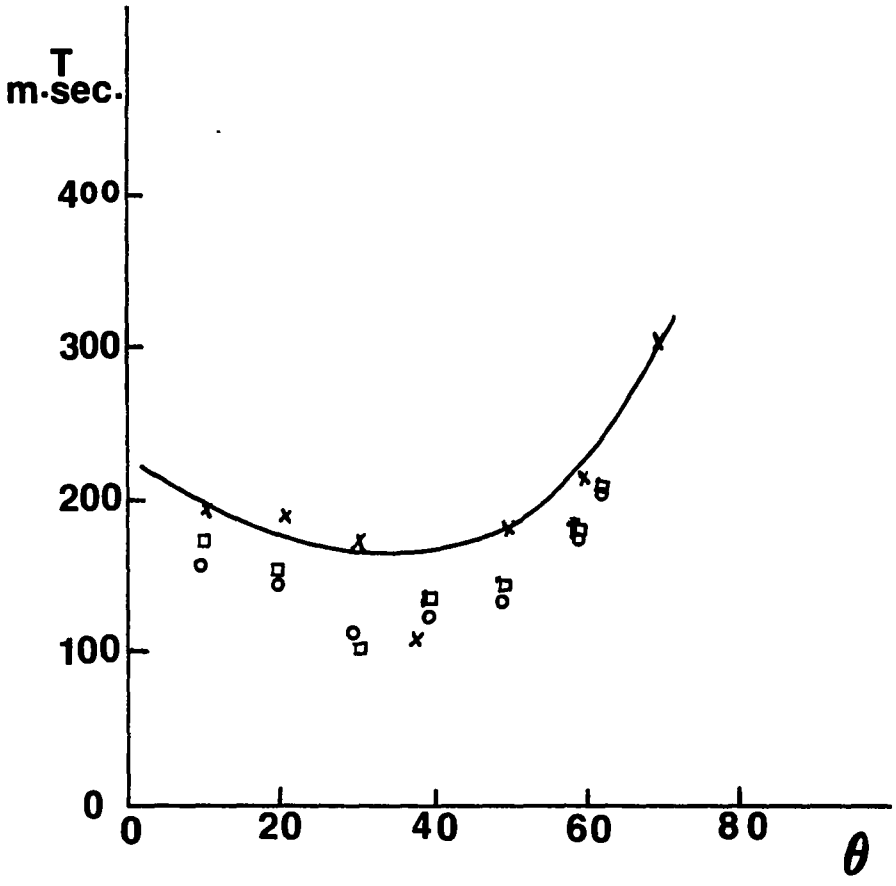

Fig. 7

Relaxation time versus θ for 2-3 transitions.

Symbols as in Fig. 6.

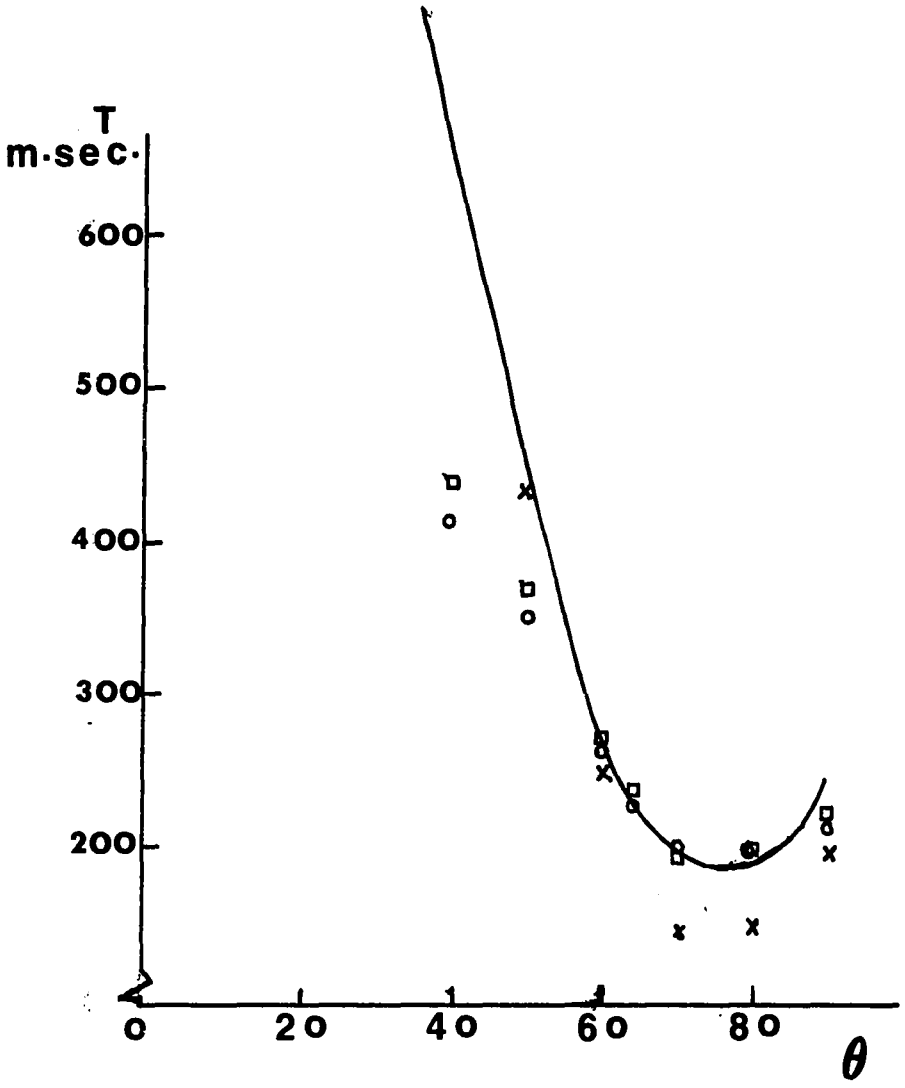

Fig. 8

Relaxation time versus θ for 3-4 transitions.

Symbols as in Fig. 6.

TABLE I

Relaxation Time Measurements

Sample	Transition measured	Angle θ	Magnetic Field K.G.	Relaxation time in m.sec.	Results from other published data
I	2-3	60°	3.66	175 ± 15	210* m.sec.
I	2-3	50°	4.17	140 ± 10	178* m.sec.
I	1-2	60°	2.06	160 ± 10	
I	1-2	40°	2.48	150 ± 8	
I	3-4	60°	2.65	270 ± 10	250* m.sec.
II	2-3	60°	3.66	166 ± 5	
II	1-2	50°	2.22	146 ± 4	
II	3-4	60°	2.65	260 ± 5	

Sample I : Cr^{3+} concentration .05% . Sample II: Cr^{3+} concentration .08%.

* Data taken from Standley and Vaughan (1965). Temperature T = 4.2°K .

IV. Experimental measurements of spin-phonon transition probabilities

IV.1 Method of measurements.

In this section, an experimental method based on the technique of microwave pumping designed to measure spin-phonon transition probabilities, will be described. Such a method was first used by Weissfloch (1967) to evaluate spin-phonon transition probabilities in potassium chromicyanide. In section II.4.3 we derived relations 2.19 and 2.20 which relate experimentally measurable quantities, population difference and single time constant, and the spin-phonon probabilities. One can change the role of saturated and measured transitions to obtain two further equations of the type 2.19 and 2.20. There are three possibilities of such combinations leading to a system of six linear equations. The resulting equation could then easily be solved for the six basic W_{ij}'s.

The method used in this work was based on the previous discussion with little modification. Instead of using two sources of microwave pump covering appropriate frequency band and the necessary instrumentation (e.g. a three-port resonant cavity to apply the three signal simultaneously), we contented ourselves with a technique requiring only one additional signal source and a

two-port cavity. The realization of suitable experimental conditions required, then, that the measurements be carried out for an orientation of the static magnetic field such that the two allowed absorption lines of the crystal have equal, or nearly equal, frequencies. Instead of the six measurements (three relaxation time measurements and three measurements of population differences, i.e. of line-heights), the experiments consisted of the following steps:

1. Measurement of $(T_R)_{21}$ and $n_2 - n_1$, by saturating 4-3 and 3-2 simultaneously with the same microwave signal.

2. Measurement of the (equivalent) relaxation time of the 2-1 transition with no pump signal applied.

3. Measurement of the relaxation time and population difference for the 2-1 transition when either 4-3 or 3-2 is saturated.

The results of steps 1 to 3 lead to a total of seven conditions to be satisfied by the six unknown and independent W_{ij}'s. Only step 1, however, leads to linear relationships, namely equations 2.19 and 2.20, therefore a high speed digital computer is necessary to evaluate the experimental data and obtain internally consistent solutions for the spin-phonon transition probabilities.

A suitable orientation of the sample of ruby, for the determination of spin-phonon transition probabilities, occurs when the angle between the static magnetic field $\vec{H}$ and the crystalline C axis of the crystal is approximately equal to 63.2^{o}.

The positions of the ground state energy levels for a constant magnitude of $\vec{H}$ (2050) as a function of the direction of $\vec{H}$, about this angle, are shown in Fig. 9(d). In Fig. 9(b), the energy levels are shown at a constant angle (63^{o}) as a function of the applied static magnetic field, similarly in Figs. 9(a) and 9(c) for angles 62^{o} and 64^{o} respectively. When $\theta = 63.2^{o}$, the two resonance lines 4-3 and 3-2 coincide at a static magnetic field of 2050 gauss, permitting their simultaneous saturation by the pump signal. By rotating the crystal by 1^{o} to either side of $\theta = 63.2^{o}$, the 4-3 and 3-2 lines are sufficiently separated to allow them to be saturated or monitored individually. The technique used to measure relaxation time was the same as the one described in section III.4. The X-band EPR spectrometer used was that described in section III.2, except for adding a pump klystron. The pump signal, delivered by a Varian X-26 B reflex klystron which covered the range 6.3000 to 7.500 GC/sec. and delivered 1 watt of power, was applied to the crystal through the non-resonant input of the two-port cavity.

The population differences under various pumping conditions were measured by recording the changes of the height of the derivative of the absorption line, which was recorded on the chart recorder. This method of measuring the population differences has the advantages of superior signal-to-noise ratio and the linearity of the system over the direct line height measurements using the oscilloscope. For the change of line height

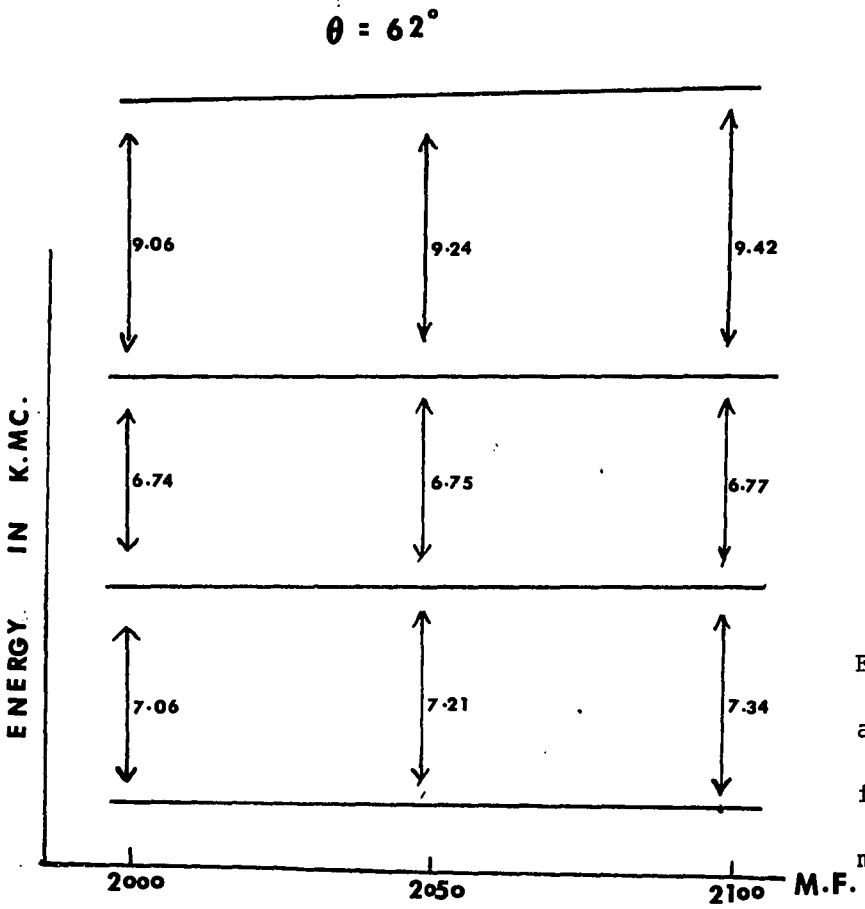

Fig. 9(a)

Energy level diagra
at angle 62° as
function of
magnetic field.

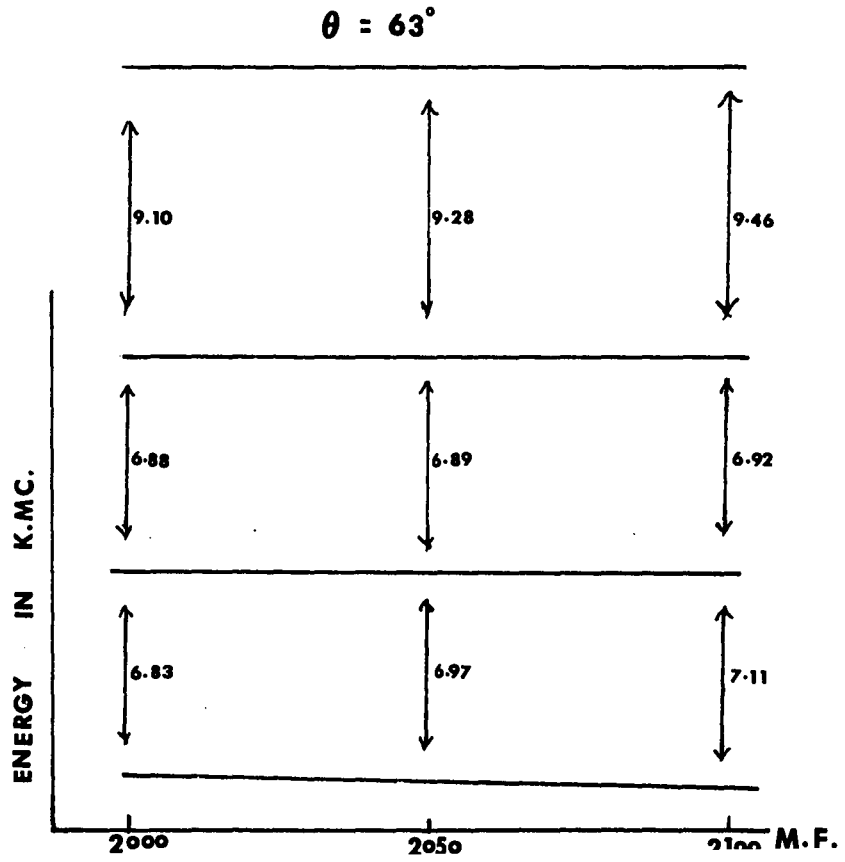

Fig. 9 (b)

Energy level diagr
at angle 63° as
function of
magnetic field.

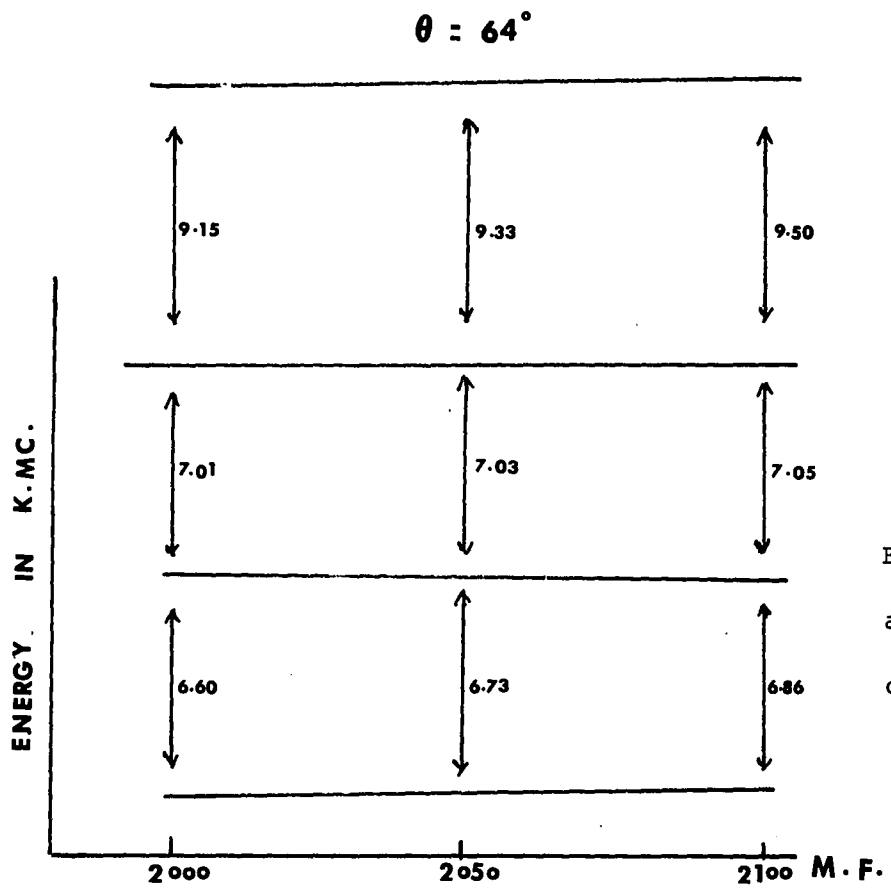

Fig. 9 (c)

Energy level diagram at angle 64° as functio of magnetic field.

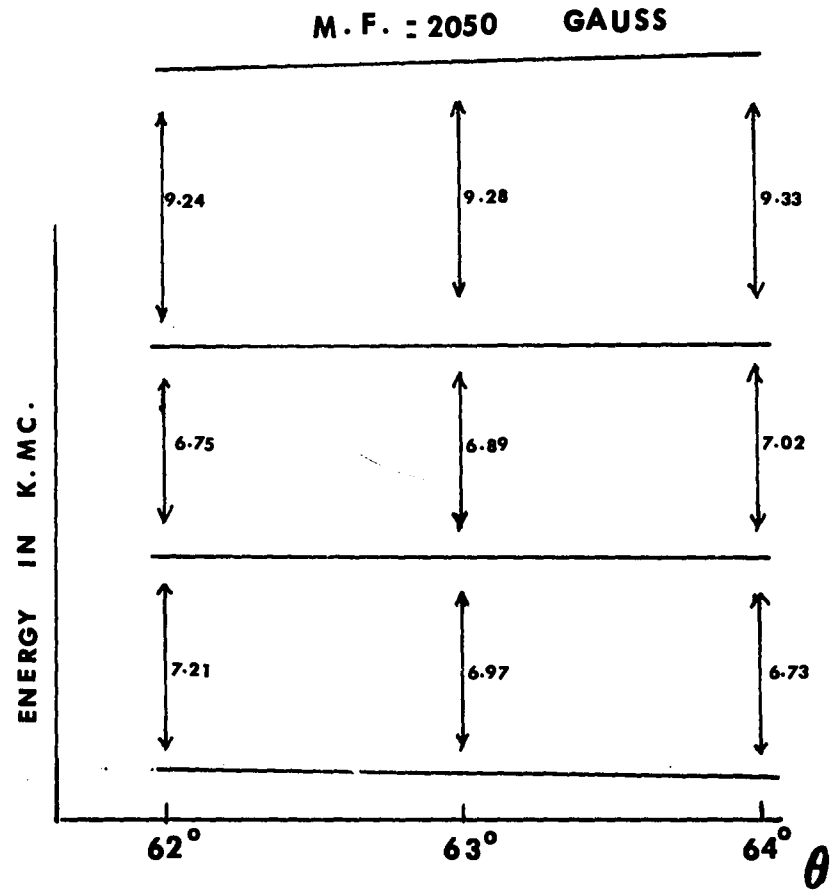

Fig. 9 (d)

Energy level diagram at 2050 Gauss as function of θ.

measurements, it was found advantageous to work with as low a Q-factor as the detected signal strength would permit. Apart from an impaired linearity of the relationship between the power absorbed by the crystal and the power reflected by the cavity, as well as an improved overall stability, the lowering of the Q-factor was used as a means to circumvent the detuning of the cavity in application of the pump power. An investigation revealed that this detuning must be due to a small temperature rise in the interior of the cavity.

Experimental adjustment of the two signal source frequencies values and orientation of the DC magnetic field was necessary to achieve a maximum change of the derivative line height. The degree of saturation of the pumped resonance line was assured from plots of the monitored line height vs. pump input power saturation and was considered to be complete when a decrease of the pump power by 6 db would produce no measureable change of the monitored line-height.

The line height observation was traced out by a slow sweep of the magnetic field through the value for which resonance is obtained. The sweep affects the resonance line which is observed and the pumped line as well. Consequently, the use of a fixed pump frequency requires that the pumped resonance line be at least as wide as the monitored one.

IV.2 Experimental results and their evaluation.

The experiments for the determination of the spin-phonon transition probabilities were carried out on two samples of Cr^{3+} concentration .05% and .08% (as analyzed by Technical Service Laboratories, Toronto, Ont.).

As explained in section IV.1, a total of seven quantities were measured. They are designated here as:

RT_1 relaxation time of 2-1 transition when no pump power is applied, angle $\theta = 63.2^{o}$

RT_2 relaxation time of 2-1 transition when transition 4-3 is saturated, angle $\theta = 62.1^{o}$

RT_3 relaxation time of 2-1 transition when transition 3-2 is saturated, $\theta = 64.5^{o}$

RT_4 relaxation time of 2-1 transition when both transitions 4-3 and 3-2 are saturated, $\theta = 63.2^{o}$

PR_2 the ratio of the dynamic equilibrium spin-population difference of transition 2-1, transition 4-3 is saturated, to its thermal equilibrium

PR_3 that ratio when transition 3-2 is saturated

PR_4 that ratio when both 4-3 and 3-2 transitions are saturated

The first six columns of Table II list the various measurements

Table II

Summary of Experimental Results, Computed Values of Relaxation Times and Ratio of Line Heights

Quantity Measured	Angle θ	Pump Frequency in GHz	Saturated Transition	Experimental Results Sample I*	Experimental Results Sample II**	Computed Values Set I	Computed Values Set II	Computed Values Set III
RT_1	63.2	-	none	170 ± 15	160 ± 15	160	155	150
RT_2	62.1	7.192	3-4	135 ± 5	130 ± 5	138.6	138.3	138.3
RT_3	64.5	7.016	2-3	142 ± 5	147 ± 5	151.6	144	148
RT_4	63.2	6.92	2-3 & 3-4	108 ± 5	106 ± 5	107.0	106.7	106.7
PR_2	62.1	7.192	3-4	1.11 ± .08	1.12 ± .08	0.947	0.942	0.949
PR_3	64.5	7.016	2-3	1.44 ± .08	1.44 ± .08	1.298	1.347	1.32
PR_4	63.2	6.92	2-3 & 3-4	2.1 ± .08	2.09 ± .08	2.095	2.05	2.069

* Sample I : Cr^{3+} content .05%

monitoring frequency = 9.3 GHz

** Sample II: Cr^{3+} content .08%

Relaxation Times T_{12} in Milliseconds

which were carried out for the direction of the magnetic field $\theta = 63.2 \pm 1^{o}$ with respect to the C-axis, and the results obtained. With the help of a computer, we attempted to find a set of spin-phonon transition probabilities for the six possible transitions which would yield the observed values of columns 5 and 6 of Table II. These "best-fit" W_{ij}'s are to be considered as "apparent" spin-phonon transition probabilities and the quality of the fit, a measure of the adequacy of the spin-lattice relaxation rate equations.

Table III lists three sets of W_{ij}'s which yielded values closest to the seven measured quantities of Table II. The corresponding computed quantities are shown in columns 7, 8, and 9 of Table II. It will be noted that these quantities fall somewhat outside the estimated experimental errors. Fig. 10 is a diagram illustrating the three computed sets and the experimentally measured values of RT1-PR4. We observed a noticeable departure of the calculated values from the measured ones for the quantities RT2, PR2 and PR3. In Table IV, our average "apparent" W_{ij}'s are compared with the W_{ij}'s (multiplied by 2) computed from the G-tensor measured by Hemphill, Donoho and McDonald (1966).

In calculating the W_{ij}'s from the G-tensor, we used the isotropic approximation for the elastic constants (Weissfloch 1966). Since the G-tensor is a fourth rank tensor, and for ruby the local symmetry of the Cr^{3} site is C_{3v}, in which case the tensor has no

TABLE III

Apparent Spin-Phonon Transition Probabilities (in sec^{-1})

W21	W31	W32	W41	W42	W43	
0.67	1.46	0.93	3.79	3.64	0.32	Set I
0.79	1.63	1.00	3.52	3.39	0.43	Set II
0.75	1.82	1.22	3.37	3.24	0.41	Set III

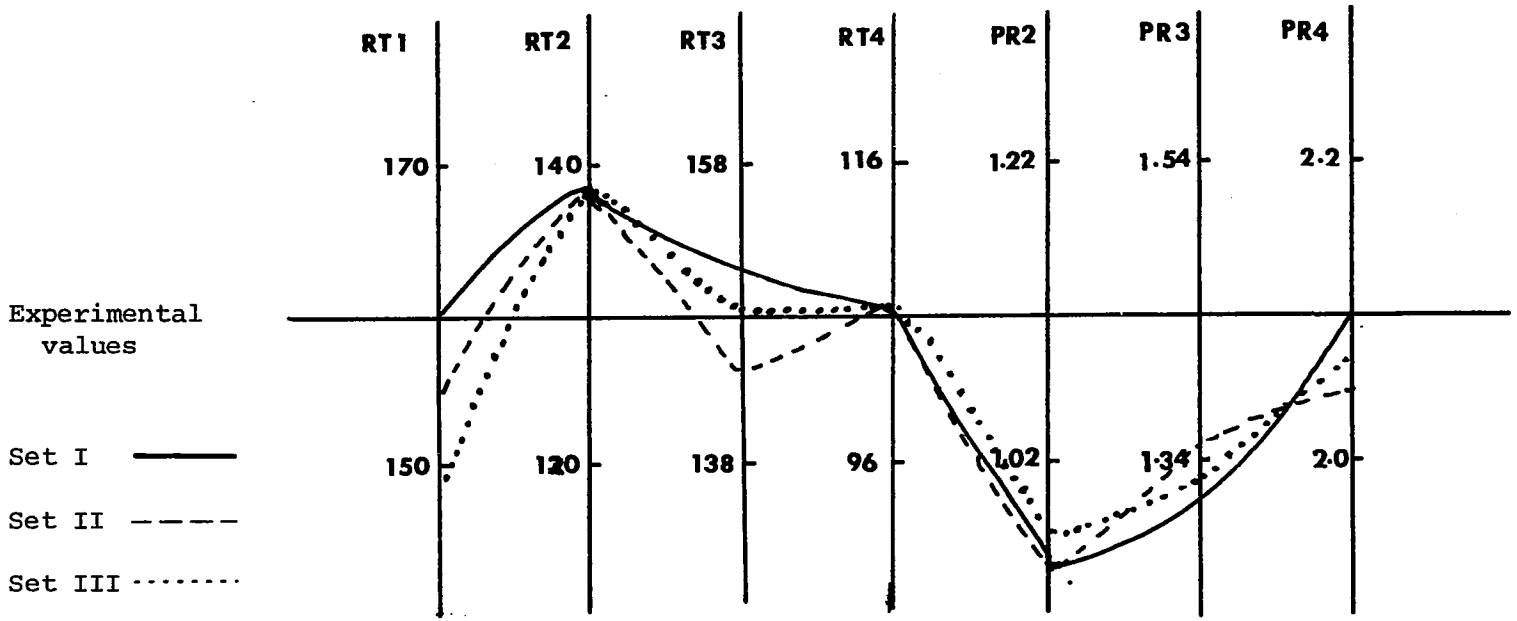

Fig. 10

Diagram illustrating 3 different computed sets and the experimentally measured values of RT1 to PR4.

TABLE IV

Average Apparent and Theoretical Spin-Phonon Transition Probabilities (in sec^{-1})

	A	B	
	This work	From G Tensor	Ratio $\frac{A}{B}$
W21	.75	.30	2.50
W31	1.51	1.46	1.03
W32	1.04	0.34	3.06
W41	3.64	2.77	1.31
W42	3.44	1.03	3.34
W43	.40	.22	1.81

axial symmetry, i.e. the tensor is not invariant for rotation by the angle θ or by the azimuthal angle ϕ. As a result, the calculated W_{ij}'s are not symmetrical about $\theta = 90^{o}$ nor about the angle ϕ. The average of the W_{ij}'s at $\theta = 63^{o}$ and $\theta = 117^{o}$ (representing the two complexes) and the average over the angle ϕ were taken.

It is interesting to consider how the application of the multipliers of column 3, Table IV, to the theoretical W_{ij}'s affects the predicted relaxation times at 9.3 GHz of the 2-3 and 3-4 transitions for the same orientation ($\theta = 63^{o}$) of the magnetic field. The resulting relaxation times are shown in Table V.

TABLE V

Effect of Multipliers on the Predicted Relaxation Times

	T_{12} msec	T_{23}/T_{12}	T_{34}/T_{12}
our measurements	170	1.18	1.35
from G-tensor	407	0.52	0.63
using W_{ij}'s from G-tensor multiplied by experimental factors from Table IV	170	0.73	1.06

V. Discussion and Conclusion

In section III.4, the results of the angular dependence of the relaxation time for the 1-2, 2-3, and 3-4 transitions at 9.3GHz were presented in Figs. 6, 7, and 8 respectively. Also shown in the figures are the experimental points of Standley and Vaughan (1965) and the effective relaxation times deduced from Donoho's computation, reduced by a factor of 2. Our measurements for the 2-3 and 3-4 transitions are seen to agree well with Standley and Vaughan's as well as with the (scaled down) theoretical curves. On the other hand, the relaxation times for the 1-2 transition, not previously reported, are seen to fall noticeably below the theoretical curve.

To investigate such discrepancy, further experimentation was conducted, the method and results of which were reported in chapter IV.

A few words should be said about the reliability of the experimental results; one might, for instance, question the value of the line height measurements for the determination of the dynamic equilibrium populations. There is no fundamental difficulty in assuring that the detection system of the spectrometer is sufficiently linear. The error margin of $\pm$ 5% for which allowance was made in the evaluation of the measurements, fully takes care of any instrumental uncertainty. A serious problem would arise if it could be proved that the width or shape of the monitored absorption

line changes due to the saturation of the other lines. We have been unable to detect any such line-shape changes, but line-shape measurements are not readily carried out with great accuracy. On the other hand, it is difficult to see what mechanism could be responsible for any phenomenon of this type.

Pump method. Possible effects of cross-relaxation.

As was mentioned on page 47, and as can be seen in Table II, the best-fit values for RT_2, PR_2 and PR_3 fall outside the estimated error of measurement. It will be immediately noticed that in the experimental conditions under which these measurements are taken, the transitions 2-3 and 3-4 are separated by only 500 MHz. One could thus expect the presence of systematic error due to cross-relaxation between these transitions. Indeed, comparison between experimental and computed values in Table II shows that the deviation is precisely in the direction which would occur if a certain degree of cross saturation had taken place. Unfortunately there exists no data for cross-relaxation at low Cr^{3+} concentration. Although Mims and McGee (1960) and Manenkov and Prokhorov (1962) showed fast cross relaxation at higher concentration, no cross relaxation was observed for Cr^{3+} concentration below .1%. Also, in the "vapour-phase" grown ruby, cross-relaxation might be expected to be smaller than that in the "verneuil" grown ruby.

In the measurements we made sure that no change in the 1-2 transition (relaxation time and line height) was obtained when the pumping power in 2-3 and 3-4 absorption lines was further increased. Nevertheless, cross-relaxation is the most plausible reason for the discrepancy between the measured and computed values of RT_2, PR_2 and PR_3. From Table IV, which lists the average "apparent" (average of "best-fit" W_{ij}'s) and theoretical spin-phonon transition probabilities, one concludes that the apparent W_{21}, W_{32} and W_{42} are considerably larger than the predicted ones. It is emphasized that our conclusion that W_{21}, W_{32} and W_{42} are larger than predicted, is mainly based on the measured values of RT_1, RT_4 and PR_4 which are not affected by cross-relaxation. Donoho's transition probabilities would give for RT_1, RT_4 and PR_4, the values

$$RT_1 = 395.5 \text{ m sec.} \qquad RT_4 = 136.4 \text{ m sec.} \qquad PR_4 = 2.162$$

whereas ours gives (computed values in Table II)

$$RT_1 = 160 \text{ m sec.} \qquad RT_4 = 107 \text{ m sec.} \qquad PR_4 = 2.095$$

Conclusion:

It can be seen from Table IV, column 3, that our results yield no single proportional constant between the measured "apparent" and the computed spin-phonon transition probabilities; the difference cannot be accounted for by any smaller than order of magnitude

adjustment of the coefficients in the G-tensor. The conclusion that other relaxation processes not related to the G-tensor play an important role, seems thus inevitable. It is interesting to consider how the application of the multipliers of column 3 of Table IV to the theoretical W_{ij}'s affects the predicted relaxation times at 9.3 GHz of the 2-3 and 3-4 transitions for the same orientation ($\theta \approx 63^{o}$) of the magnetic field. The resulting computed relaxation times are shown in Table V. The agreement between the predicted and measured relative magnitudes, T_{23}/T_{12} and T_{34}/T_{12}, is seen to be appreciably improved by this operation. This observation lends some additional weight to the results of Table IV, which shows that W_{21}, W_{32} and W_{42} appear considerably enhanced. This enhancement is attributed to the presence of other relaxation mechanisms.

VI. Bibliography

Bleaney, B. and Stevens, K. W. H. 1953. Rep. on Progr. in Phys. 16, 108.

Bloembergen, M., Shapiro, S., Pershan, P.S., and Artman, S.O. 1959. Phys.Rev. 114, 445.

Bloembergen, M., Purcell, E.M, and Pound, R.V. 1948. Phys.Rev. 73, 679.

Bowers, K.D. and Owen, J. 1955. Rep. on Progr. in Phys. 18, 304.

Bowers, K.D. and Mims, W.B. 1959. Phys.Rev. 115, 285.

Carruthers, J.A. and Rumin, N.C. 1965. Can.J.Phys. 43, 576.

Chang, W.S. and Siegman, A.E. 1958. Electron Tube. Laboratory Tech.Repts.No.156-2, Stanford Electronics Labs., Stanford, California.

Donoho, P.L. 1964. Phys.Rev. 133 A, 1080.

Donoho, P.L. and Hemphill, R.B. 1962. Bull Am.Phys.Soc. 7, 306.

Feher, G. 1957. Bell Syst.Tech.Jour. 36, 449.

Gorter, C.J. 1947. "Paramagnetic Relaxation" Elsevie, Amsterdam and New York.

Geusic, J.E. 1956. Phys.Rev. 102, 1252.

Hemphill, R.B., Donoho, P.L. and McDonald, E.D. 1966. Phys.Rev. 146, 329.

Kronig, R. de L. 1939. Physica 6, 33.

Lees, R.A., Moore, W.S. and Standley, K.J. 1967. Proc. Phys. Soc. 91, 105.

Manenkov, A.A. and Prokhorov, A.M. 1955. J.E.T.P. 28, 762.

Manenkov, A.A. and Prokhorov, A.M. 1962. J.E.T.P. 14, 317.

Mims, W.B. and McGee, J.D. 1960. Phys.Rev. 119, 1233.

Poole, C.P. 1967. Electron Spin Resonance (Interscience Publishers, N.Y.)

Pound, R.V. 1947. Proc. IRE 35, 1405.

Schulz-DuBois, E.O. 1959. Bell System Tech. J.

Shiren, N.S. and Tucker, E.B. 1961. Phys.Rev.Letters 6, 105.

Shiren, N.S. 1962. Bull. Am. Phys. Soc. Sec.II, 7, 29.

Standley, K.J. and Vaughan, R.A. 1965. Phys.Rev.139, A 1275.

Stevens, K.W.H. 1967. Rep. on Progr. inPhys. 30, 189.

Tucker, E.B. 1961. Phys.Rev.Letters 6, 183.

Van Vleck, J.H. 1940. Phys.Rev.57, 426.

Watkins, G.D. and Feher, E.R. 1962. Bull. Am. Phys.Soc.Ser.II, 7, 29.

Weissfloch, C.F. 1964. M.Sc. Thesis, Department of Physics, McGill University.

Weissfloch, C.F. 1966. Ph.D. Thesis, Department of Physics, McGill University.

Weissfloch, C.F. 1967. Can.J.Phys. 45, 3269.

Zaripov, M.M., Shamonin, Y.Y. 1956. J.E.T. p., 3, 171.